PCCP

PAPER

View Article Online
View Journal | View Issue

Cite this: *Phys. Chem. Chem. Phys.*, 2017, **19**, 30351

The intrinsic basicity of the phosphate backbone exceeds that of uracil and thymine residues: protonation of the phosphate moiety is preferred over the nucleobase for pdThd and pUrd†

R. R. Wu,[a] L. A. Hamlow,[a] C. C. He,[a] Y.-w. Nei,[a] G. Berden,[b] J. Oomens[b] and M. T. Rodgers*[a]

The gas-phase conformations of the protonated forms of thymidine-5′-monophosphate and uridine-5′-monophosphate, $[pdThd+H]^+$ and $[pUrd+H]^+$, are investigated by infrared multiple photon dissociation (IRMPD) action spectroscopy and electronic structure calculations. The IRMPD action spectra of $[pdThd+H]^+$ and $[pUrd+H]^+$ are measured over the IR fingerprint and hydrogen-stretching regions using the FELIX free electron laser and an OPO/OPA laser system. Low-energy conformations of $[pdThd+H]^+$ and $[pUrd+H]^+$ and their relative stabilities are computed at the MP2(full)/6-311+G(2d,2p)//B3LYP/6-311+G(d,p) and B3LYP/6-311+G(2d,2p)//B3LYP/6-311+G(d,p) levels of theory. Comparisons of the measured IRMPD action spectra and B3LYP/6-311+G(d,p) linear IR spectra computed for the low-energy conformers indicate that the dominant conformers of $[pdThd+H]^+$ and $[pUrd+H]^+$ populated in the experiments are protonated at the phosphate oxo oxygen atom, with a *syn* nucleobase orientation that is stabilized by strong P=OH$^+$···O2 and P–OH···O4′ hydrogen-bonding interactions, and C2′-*endo* sugar puckering. Minor abundance of conformers protonated at the O2 carbonyl of the nucleobase residue may also contribute for $[pdThd+H]^+$, but do not appear to be important for $[pUrd+H]^+$. Comparisons to previous IRMPD spectroscopy investigations of the protonated forms of thymidine and uridine, $[dThd+H]^+$ and $[Urd+H]^+$, and the deprotonated forms of pdThd and pUrd, $[pdThd-H]^-$ and $[pUrd-H]^-$, provide insight into the effects of the phosphate moiety and protonation on the conformational features of the nucleobase and sugar moieties. Most interestingly, the thymine and uracil nucleobases remain in their canonical forms for $[pdThd+H]^+$ and $[pUrd+H]^+$, unlike $[dThd+H]^+$ and $[Urd+H]^+$, where protonation occurs on the nucleobases and induces tautomerization of the thymine and uracil residues.

Received 13th August 2017,
Accepted 24th October 2017

DOI: 10.1039/c7cp05521h

rsc.li/pccp

Introduction

Both thymine and its RNA analogue uracil are subject to tautomerization under certain conditions. A number of studies have examined the intrinsic properties of the protonated forms of thymine (Thy) and uracil (Ura), and their respective nucleoside analogues, thymidine (dThd) and uridine (Urd).[1–8] All of these studies found that protonation induces tautomerization of Thy and Ura for both the isolated nucleobases and their nucleoside analogues. The 2,4-dihydroxy tautomers of protonated Thy and Ura are found to be the most stable forms in the gas phase.[1–5] Tautomerization as well as the flexibility of the hydroxyl substituents leads to a large variety of conformations of $[dThd+H]^+$ and $[Urd+H]^+$ coexisting in the gas phase.[6–8] Keto–enol tautomeric shifts of the Thy and Ura nucleobases that may occur during DNA replication could lead to mutations and nucleobase mispairing.[9,10] A previous study that examined the N–glycosidic bond stabilities of the protonated Ura nucleosides found that protonation, and further tautomerization, lower the activation barriers for N–glycosidic bond cleavage of Urd and 2′-deoxyuridine (dUrd).[11] Parallel behavior is found for the analogous Thy nucleosides, dThd and 5-methyluridine (Thd), currently under investigation in our laboratory. Thus, both protonation and tautomerization exert a strong influence on the N–glycosidic bond stabilities of the Thy and Ura nucleosides. In contrast, the glycosidic bond stabilities of the other canonical DNA and RNA nucleosides are strongly influenced by protonation,[12–14] but not

[a] *Department of Chemistry, Wayne State University, Detroit, Michigan 48202, USA. E-mail: mrodgers@chem.wayne.edu; Tel: +1-313-577-2431*
[b] *Radboud University, Institute for Molecules and Materials, FELIX Laboratory, Toernooiveld 7c, 6525 ED, Nijmegen, The Netherlands*

† Electronic supplementary information (ESI) available. See DOI: 10.1039/c7cp05521h

tautomerization. Clearly, the structural and thermochemical properties of Thy and Ura nucleobases and nucleosides are greatly influenced by tautomerization.

Phosphorylation of dThd or Urd at the 5′-hydroxyl gives thymidine-5′-monophosphate (pdThd) or uridine-5′-monophosphate (pUrd), respectively. Previously, studies to characterize the gas-phase conformations of the deprotonated forms of these nucleotides, $[pdThd-H]^-$ and $[pUrd-H]^-$,[15,16] as well as Pb^{2+} complexed with $[pUrd-H]^-$, $[pUrd-H+Pb]^+$,[17] have been carried out using infrared multiple photon dissociation (IRMPD) action spectroscopy. In the stable gas-phase conformations of $[pdThd-H]^-$ and $[pUrd-H]^-$, the Thy and Ura nucleobases remain in their canonical forms. For both structures, the deprotonated phosphate moiety is stabilized by a strong hydrogen-bonding interaction with the 3′-hydroxyl substituent, and a weak noncanonical hydrogen-bonding interaction with the C5–H hydrogen atom. These intramolecular interactions lead to an anti nucleobase orientation and C3′-*endo* sugar puckering. In contrast, when Pb^{2+} complexes with $[pUrd-H]^-$, it strongly binds to the phosphate and carbonyl moieties of Ura, leading to compactly folded structures. A mixture of keto and enolic forms of $[pUrd-H+Pb]^+$ are populated in the experiments, indicating that the metal binding interaction facilitates tautomerization of the Ura moiety. However, little is known about the intrinsic properties of the protonated forms of the pdThd and pUrd mononucleotides.[18] IRMPD action spectroscopy techniques assisted by complementary theoretical calculations have proven to be a powerful means of elucidating the intrinsic structural behavior of nucleic acid building blocks in various local environments of differing pH and ionic strength by examining their associated deprotonated,[15,16,19,20] protonated[5,7,8,21–34] and sodium (or other metal) cationized forms.[35–49] This technique is very helpful for elucidating intrinsic structural features of nucleic-acid constituents, in particular, the preferred site(s) of protonation or metal cation binding as well as tautomerization of the nucleobase are generally readily deduced along with the nucleobase orientation, sugar puckering, and the presence of intramolecular hydrogen bonds.

Therefore, here we investigate the gas-phase conformations of protonated thymidine-5′-monophosphate, $[pdThd+H]^+$, and protonated uridine-5′-monophosphate, $[pUrd+H]^+$ using IRMPD action spectroscopy techniques combined with theoretical modeling. Comparison of the stable gas-phase conformations of $[pdThd+H]^+$ and $[pUrd+H]^+$ to those of $[pdThd-H]^-$ and $[pUrd-H]^-$[15,16] allows the effect of pH (*i.e.*, protonation) on the structures of pdThd and pUrd to be determined. Comparison of the stable gas-phase conformations of $[pdThd+H]^+$ and $[pUrd+H]^+$ to those of protonated thymidine and uridine, $[dThd+H]^+$ and $[Urd+H]^+$,[7,8] allows the effect of phosphate moiety on the structures to be elucidated. As a large variety of 2,4-dihydroxy tautomers of $[dThd+H]^+$ and $[Urd+H]^+$ as well as minor abundances of O2 protonated conformers of $[dThd+H]^+$ and O4 protonated conformers of $[Urd+H]^+$ are present in the experiments, it is of great interest to reveal the influence of the phosphate moiety on the preferred site(s) of protonation and tautomerization of dThd and Urd. Present IRMPD action spectroscopy results for $[pdThd+H]^+$ are also compared to results obtained from combined ion-mobility spectrometry mass spectrometry (IMS MS) studies of $[pdThd+H]^+$ previously reported.[19]

Experimental and computational methods

IRMPD action spectroscopy experiments

The IRMPD action spectra of $[pdThd+H]^+$ and $[pUrd+H]^+$ were measured over the IR fingerprint and hydrogen-stretching regions using a Fourier transform ion cyclotron resonance mass spectrometer (FT-ICR MS)[50–52] coupled to a widely-tunable free electron laser (FEL)[53] or an OPO/OPA laser system. The mononucleotides, pdThd and pUrd, were purchased from Sigma-Aldrich (Zwijndrecht, the Netherlands). Approximately 1 mM pdThd or pUrd and 20 mM HCl were dissolved in 50% : 50% $MeOH/H_2O$ solutions. The solutions were delivered to a Micromass "Z-spray" electrospray ionization (ESI) source at a flow rate of ~4.0–5.5 μL min^{-1}. Ions were accumulated in an rf hexapole ion trap for several seconds to affect efficient thermalization of the ions prior to pulsed extracted through a quadrupole deflector. The ions were guided through a 1 m long rf octopole into the FT-ICR MS and stored in the ICR cell to cool to room temperature by radiative emission.[51] The protonated mononucleotides, $[pdThd+H]^+$ and $[pUrd+H]^+$, were isolated using stored waveform inverse Fourier transform (SWIFT) techniques and irradiated for 2–3 s by the FEL (10 pulses per s with 15–50 mJ per pulse) or 3–4 s by the OPO/OPA laser system (10 pulses per s with 10–20 mJ per pulse) to induce IR photodissociation over the IR fingerprint (~550–1900 cm^{-1}) and hydrogen-stretching (~3300–3800 cm^{-1}) regions, respectively.

Theoretical calculations

The chemical structures of neutral pdThd and pUrd are displayed in Fig. 1. All favorable protonation sites were investigated: O2, O4, 2,4-dihydroxy tautomers, and the phosphate oxo oxygen atom. 300 candidate structures for each site of protonation and tautomeric form of the nucleobase were generated by simulated annealing using HyperChem software[54] with the

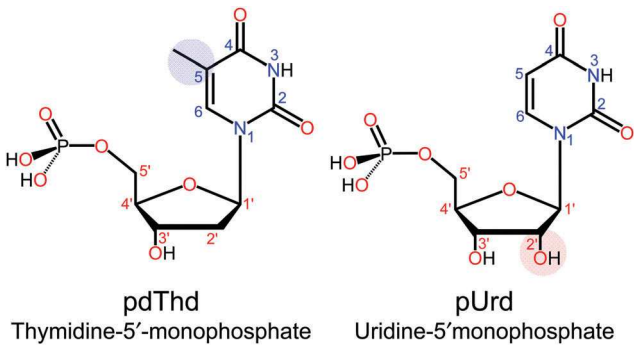

Fig. 1 Chemical structures of neutral thymidine-5′-monophosphate (pdThd) and uridine-5′-monophosphate (pUrd). The numbering of the nucleobase and sugar moieties is also shown; the 5-methyl and 2′-hydroxyl substituents that differentiate these nucleotides are shaded in blue and red, respectively.

Amber 2 force field. The simulated annealing procedure employed in the current study has been described in detail previously.[7,8,28,30,31] Geometry optimizations, frequency analyses, and single point energy calculations of 20–30 candidate structures (including different combinations of nucleobase orientation and sugar puckering) for each protonation site were performed using the Gaussian 09 suite of programs.[55] All candidate structures were first optimized at the B3LYP/6-31G(d) level of theory to facilitate convergence, and then re-optimized using a larger basis set, 6-311+G(d,p), to improve the description of the intramolecular hydrogen-bonding interactions. Frequency analyses were also performed using the 6-311+G(d,p) basis set to generate calculated IR spectra. Single point energies were calculated at the MP2(full) and B3LYP levels of theory using the 6-311+G(2d,2p) basis set including zero-point energy (ZPE) and thermal corrections to 298 K. Due to the significant anharmonicity of the vibrational modes of the phosphate moiety, scaling factors between 0.98 and 1.07 have been shown to be needed to bring the computed frequencies into agreement with measured values.[15,16,56–62] In this work, the frequencies below ~1350 cm^{-1} (shown in red in the calculated spectra) are left unscaled to best reproduce the measured bands associated with the phosphate moiety. A scaling factor of 0.985 is applied to the frequencies above ~1350 cm^{-1} in the IR fingerprint region (shown in blue), whereas a scaling factor of 0.958 is used for the hydrogen-stretching region (shown in green). In addition, the calculated vibrational frequencies are convoluted with a 20 cm^{-1} fwhm Gaussian line shape for the IR fingerprint region, and 10 cm^{-1} Gaussian line shape for the hydrogen-stretching region, to reproduce the experimental broadening of the measured IRMPD profiles.

To further assess the relative stabilities of the stable low-energy conformations of $[pdThd+H]^+$ and $[pUrd+H]^+$ in the gas phase *versus* aqueous environments, single point energies of select low-energy conformers were also calculated at the B3LYP/6-311+G(2d,2p) and MP2(full)/6-311+G(2d,2p) levels of theory in a polarizable continuum using the integral equation formalism variant (IEFPCM) available in Gaussian 09.[55]

Results

IRMPD action spectroscopy

Photodissociation of $[pdThd+H]^+$ and $[pUrd+H]^+$ was induced by the FELIX free electron laser or an OPO/OPA laser system. The photodissociation products formed arise primarily from phosphate ester and glycosidic bond cleavage processes. Ionic products at m/z = 207 and 81, corresponding to $[Thy+H_2PO_3]^+$ and $H_2PO_3^+$, respectively, are observed for $[pdThd+H]^+$. As the nucleobase and phosphate moieties of pdThd are not covalently bound, the former product is likely a hydrogen-bound species that undergoes sequential dissociation to produce the $H_2PO_3^+$ product. Theoretical and spectroscopy results discussed later establish the importance of hydrogen-bonding in the structures of $[pdThd+H]^+$ accessed in the experiments. Ionic products at m/z = 213 and 97, corresponding to $[pUrd-Ura+H]^+$ and $[pUrd-Ura-H_3PO_4-H_2O+H]^+$ (the latter ionic product has a chemical formula of $C_5H_5O_2^+$), respectively, are observed for $[pUrd+H]^+$. The photodissociation behaviors of $[pdThd+H]^+$ and $[pUrd+H]^+$ are quite distinct from those of the other protonated DNA and RNA mononucleotides, where glycosidic bond cleavage producing the protonated nucleobase is the dominant photodissociation pathway observed.[31,32,34]

The ratio of the total fragment ion intensity to that of the protonated mononucleotide, $[pNuo+H]^+ = [pdThd+H]^+$ or $[pUrd+H]^+$, determine the IRMPD yield at each irradiation frequency according to eqn (1),

$$\text{IRMPD yield} = \sum_i I_{\text{fragment}_i} \Big/ \left(\sum_i I_{\text{fragment}_i} + I_{[p\text{Nuo}+H]^+} \right) \quad (1)$$

The IRMPD yield was corrected for variations in the laser power as a function of the wavelength of the FEL or OPO laser using linear scaling. IRMPD action spectra of $[pdThd+H]^+$ and $[pUrd+H]^+$ were measured over the ranges extending from ~550 to 1900 cm^{-1} and ~3300 to 3800 cm^{-1} and are compared in the top panel of Fig. 2. The IRMPD action spectra acquired over the hydrogen-stretching region for $[pdThd+H]^+$ and $[pUrd+H]^+$ are very crucial for elucidating the gas-phase conformations as the IR bands measured over the FELIX region are very broad and poorly resolved, and indeed span much of the fingerprint region. Such extensive broadening approaching continuum behavior has been seen in other IRMPD and IRPD (tagging) studies where the conformers populated in the experiments have strong hydrogen-bonding interactions

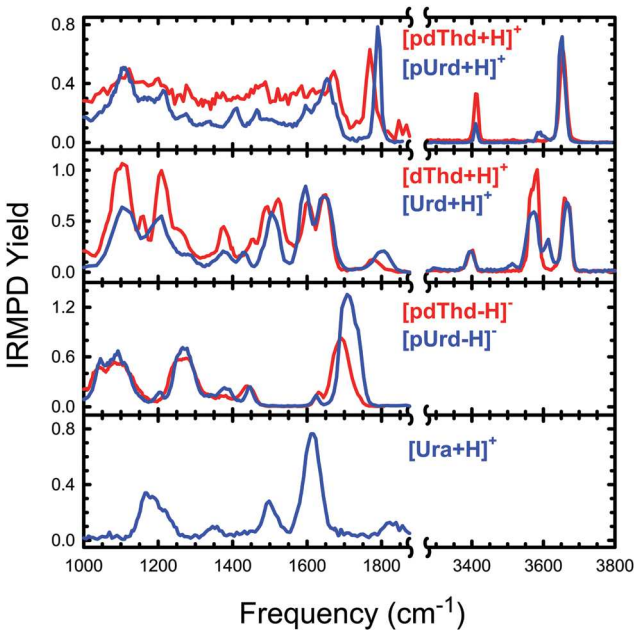

Fig. 2 IRMPD action spectra of the protonated forms of the thymidine and uridine nucleosides, $[dThd+H]^+$ and $[Urd+H]^+$, the protonated and deprotonated forms of the thymidine and uridine nucleotides, $[pdThd+H]^+$, $[pUrd+H]^+$ $[pdThd-H]^-$, and $[pUrd-H]^-$ and the protonated form of uracil, $[Ura+H]^+$. Results for $[dThd+H]^+$ are taken from ref. 7, those for $[Urd+H]^+$ from ref. 8, those for $[pdThd-H]^-$ from ref. 15, those for $[pUrd-H]^-$ from ref. 16 and those for $[Ura+H]^+$ from ref. 4.

that greatly increase the anharmonicity of the vibrational modes of the associated atoms.[63–66]

Theoretical results

The MP2(full)/6-311+G(2d,2p) and B3LYP/6-311+G(2d,2p) relative enthalpies and Gibbs free energies at 0 and 298 K of the unique stable low-energy conformers of $[pdThd+H]^+$ and $[pUrd+H]^+$ computed are summarized in Table 1. These low-energy conformers along with their relative free energies at 298 K computed at both the MP2(full) and B3LYP levels of theory are shown in Fig. S1 and S2 of the ESI.† The low-energy conformers include all combinations of the favorable states of protonation, nucleobase orientations, and sugar puckering found. The nomenclature chosen to differentiate the various low-energy conformers found is based on the state of protonation, P (phosphate oxo oxygen atom), O2, O4 and T (2,4-dihydroxy tautomeric form) followed by a capital letter (A, B, C, D, E, *etc.*) when highly parallel conformers are found for both $[pdThd+H]^+$ and $[pUrd+H]^+$. Unique conformations found only for $[pUrd+H]^+$ are designated using a lowercase Roman numeral following the site of protonation (**Pi**, **Ti**, **O4i** and **O2i**, *etc.*).

Table 1 Relative enthalpies and free energies at 0 and 298 K in kJ mol^{-1} of the stable low-energy conformers of $[pdThd+H]^+$ and $[pUrd+H]^+$[a]

		MP2(full)			B3LYP		
Species	Conformer	ΔH_0	ΔH_{298}	ΔG_{298}	ΔH_0	ΔH_{298}	ΔG_{298}
$[pdThd+H]^+$	**PA**	**0.0**	**0.0**	**0.0**	**0.0**	**0.0**	0.7
	PB	1.8	2.4	0.2	1.2	1.7	0.3
	PC	14.3	15.5	10.6	3.0	4.2	**0.0**
	PD	9.3	8.6	11.1	12.7	12.0	15.2
	TA	13.7	14.8	11.7	5.7	6.7	4.3
	PE	14.5	15.6	11.7	7.3	8.4	5.2
	TB	19.2	21.6	11.8	14.6	17.1	7.9
	PF	17.0	18.4	12.4	6.3	7.7	2.3
	O2A	17.1	18.3	13.0	6.3	7.6	2.9
	TC	15.3	15.9	14.4	9.2	9.9	9.0
	O4A	26.8	29.7	18.7	13.8	16.7	6.4
	O4B	32.5	35.6	24.8	16.9	19.9	9.8
$[pUrd+H]^+$	**Pi**	**0.0**	**0.0**	**0.0**	0.9	0.4	3.9
	Pii	1.5	2.0	0.2	1.8	1.8	3.5
	PA	3.9	3.7	4.2	3.8	3.1	7.0
	PB	5.8	6.0	5.0	5.1	4.9	7.3
	PC	9.1	10.1	6.0	0.1	0.7	**0.0**
	TA	8.2	8.6	7.3	**0.0**	**0.0**	2.1
	Piii	12.8	13.8	9.7	2.2	2.8	2.2
	Piv	13.5	14.7	10.8	7.8	8.5	8.1
	PD	9.9	9.0	11.9	11.4	10.1	16.5
	PE	16.0	17.2	13.0	8.4	9.1	8.1
	TB	19.7	21.8	13.1	8.8	9.5	8.8
	Ti	14.4	14.9	13.4	11.9	13.6	8.4
	TC	14.0	14.3	13.7	4.9	4.9	6.9
	Pv	9.8	10.4	14.6	6.4	6.3	9.2
	PF	19.2	20.2	15.8	8.6	9.1	8.2
	Tii	22.1	24.3	15.9	17.1	18.9	14.0
	O4A	25.0	27.6	18.1	10.5	12.6	6.5
	O4B	29.8	32.4	23.3	15.1	17.3	11.6
	O4i	29.8	32.3	23.5	17.4	19.5	14.2
	Tiii	29.5	29.7	27.5	19.7	19.4	20.8
	O2i	42.0	42.5	39.1	32.1	32.2	32.2

[a] Single point energy calculations using the B3LYP/6-311+G(d,p) optimized structures are performed at the MP2(full)/6-311+G(2d,2p) and B3LYP/6-311+G(2d,2p) levels of theory and include ZPE and thermal corrections.

The lowest energy conformers of $[pdThd+H]^+$ and $[pUrd+H]^+$ found depend upon the level of theory employed. MP2 favors conformers of $[pdThd+H]^+$ (*e.g.*, **PA** and **PB**) and $[pUrd+H]^+$ (*e.g.*, **Pi**, **Pii**, **PA** and **PB**) that are protonated at the phosphate oxo oxygen atom, with *syn* oriented Thy and Ura nucleobases in their canonical forms that are stabilized by strong P=$OH^+\cdots$O2 and P–OH$\cdots$O4′ hydrogen-bonding interactions, and C2′-*endo* sugar puckering. The **PA** *versus* **PB** conformers of $[pdThd+H]^+$ and $[pUrd+H]^+$, and **Pi** *versus* **Pii** conformers of $[pUrd+H]^+$ are merely rotamers of one another and differ in the rotation of the free phosphate hydroxyl. Similarly, the **Pi** and **PA** as well as the **Pii** and **PB** conformers of $[pUrd+H]^+$ are sugar hydroxyl rotamers of one another. In contrast, B3LYP favors the **PC** conformers of $[pdThd+H]^+$ and $[pUrd+H]^+$ that are protonated at the phosphate oxo oxygen atom, with *syn* oriented Thy and Ura nucleobases in their canonical forms that are stabilized by a single strong P=$OH^+\cdots$O2 hydrogen bond, and C3′-*endo* sugar puckering. The **TA** conformers of $[pdThd+H]^+$ and $[pUrd+H]^+$ exhibit C3′-*endo* sugar puckering with the protonated nucleobases in a 2,4-dihydroxy tautomeric form. The nucleobases in the **TA** conformers are also rotated in a *syn* orientation to form a strong $O2H^+\cdots$O=P hydrogen-bonding interaction. The **TA** conformers of $[pdThd+H]^+$ and $[pUrd+H]^+$ are predicted to be 7.0 kJ mol^{-1} (MP2) and 2.0 kJ mol^{-1} (B3LYP) less stable than their respective ground conformers. The most stable O4 protonated conformers, **O4A**, of $[pdThd+H]^+$ and $[pUrd+H]^+$ adopt an anti nucleobase orientation and C2′-*endo* sugar puckering. The **O4A** conformers of $[pdThd+H]^+$ and $[pUrd+H]^+$ are predicted to be 18.0 kJ mol^{-1} (MP2) and 6.0 kJ mol^{-1} (B3LYP) less stable than their respective ground conformers. The **O2A** conformer of $[pdThd+H]^+$ exhibits a *syn* nucleobase orientation and C2′-*endo* sugar puckering, which is 13.0 kJ mol^{-1} (MP2) and 2.9 kJ mol^{-1} (B3LYP) higher in free energy than the ground **PA** conformer. However, no low-energy O2 protonated conformers analogous to **O2A** of $[pdThd+H]^+$ are found for $[pUrd+H]^+$. Attempts to compute stable O2 protonated structures for $[pUrd+H]^+$ always converged to phosphate protonated structures during optimization. Clearly, the 5-methyl substituent of pdThd enhances the proton affinity of the nucleobase *versus* that of pUrd, consistent with the proton affinities reported for the isolated nucleobases.[67] In summary, P conformers of $[pdThd+H]^+$ and $[pUrd+H]^+$ are preferred over T, O4 and O2 conformers, and more so by MP2 than B3LYP.

The MP2(full)/6-311+G(2d,2p) and B3LYP/6-311+G(2d,2p) relative enthalpies and Gibbs free energies at 0 and 298 K of select low-energy conformers of $[pdThd+H]^+$ and $[pUrd+H]^+$ computed in a polarizable continuum are summarized in Table S1 (ESI†). As found for the isolated species, the lowest energy conformers of $[pdThd+H]^+$ and $[pUrd+H]^+$ computed using the IEFPCM polarizable continuum model remain conformers protonated at the phosphate moiety, *i.e.*, the **PA** and **PB** conformers of $[dThd+H]^+$ and the **PA**, **PB**, and **PC** conformers of $[dUrd+H]^+$. Indeed, conformers involving canonical forms of the nucleobase protonated at the O2 or O4 positions as well as conformers involving a minor tautomeric form of the nucleobase are destabilized relative to the **PA**–**PC**

conformers by 11.8–12.4, 4.3–12.9, and 16.2–25.8 kJ mol^{-1}, respectively.

Discussion

Experimental conformations of [pdThd+H]$^+$

The measured IRMPD and calculated IR spectra of the most representative stable low-energy conformers for each favorable state of protonation, **PA**, **PB**, **PC**, **TA**, **O2A** and **O4A** of [pdThd+H]$^+$ are compared in Fig. 3 over the IR fingerprint and hydrogen-stretching regions. The calculated IR bands that exhibit obvious disagreement with the measured IR bands are highlighted. The IR spectrum predicted for the **PA** and **PB** conformers exhibit excellent agreement with the measured IRMPD spectrum, confirming the presence of these conformers in the experiments. Comparison of the IR spectra for **PA** and **PB** indicates that the IRMPD spectral features are insensitive to the phosphate hydroxyl orientation. The calculated IR spectrum of the **O2A** conformer of [pdThd+H]$^+$ agrees reasonably well with the measured spectrum above 1600 cm^{-1}. However, the IR features predicted for **O2A** below 1200 cm^{-1} are much more intense than those at higher vibrational frequencies, whereas the opposite is true of the measured IRMPD spectrum suggesting that if present, the **O2A** conformer is likely of minor abundance. The band predicted at 1554 cm^{-1} for the **PC** conformer (dotted line) is expected to be highly anharmonic as a result of the excess proton oscillating between the phosphate oxo and O2 carbonyl oxygen atoms. As a result, it is predicted to be extremely strong, whereas experimentally such highly anharmonic modes are typically red-shifted, spread over a broad range of frequencies, and appear weak in the action spectrum,[68–70] and therefore this vibrational mode is not diagnostic. The calculated band at 3640 cm^{-1} and its small shoulder to the blue at 3680 cm^{-1} of the **PC** conformer exhibits obvious disagreement with the measured band at 3652 cm^{-1}. The calculated band at 3581 cm^{-1} of the **TA** conformer is not observed in the measured spectrum. In addition, the IR feature predicted at 3685 cm^{-1} for **TA** would broaden the measured band at 3652 cm^{-1} if **TA** was populated. The calculated bands at 1804 and 3668 cm^{-1} of the **O4A** conformer are shifted to higher frequencies relative to the measured bands at 1768 and 3652 cm^{-1}, respectively. Therefore, the **PC**, **TA** and **O4A** conformers are not present in significant abundance the experiments. The measured IRMPD and calculated IR spectra of

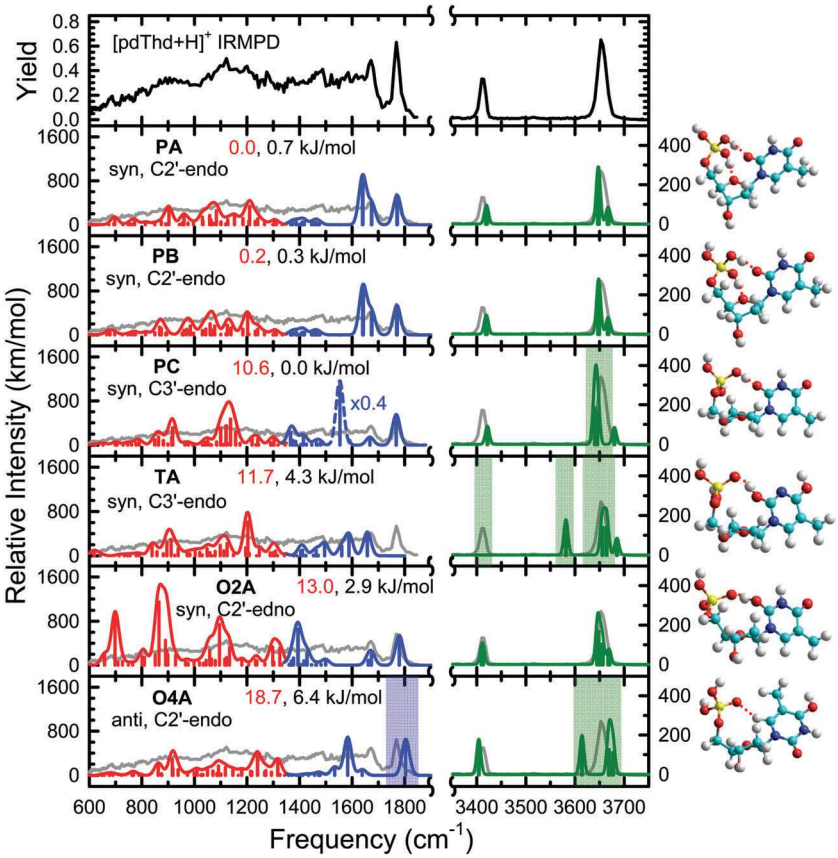

Fig. 3 Comparison of the measured IRMPD action spectrum of [pdThd+H]$^+$ with the calculated IR spectra of the ground and most stable conformers for each protonation site/tautomeric form of [pdThd+H]$^+$ and the corresponding B3LYP/6-311+G(d,p) optimized structures. Also shown are the MP2(full)/6-311+G(2d,2p) (in red) and B3LYP/6-311+G(2d,2p) (in black) relative Gibbs free energies at 298 K. The site of protonation/tautomeric form, nucleobase orientation and sugar puckering are also indicated for each conformer. To facilitate comparison of the measured and calculated spectra, the IRMPD spectrum is overlaid (in grey) with each calculated spectrum and scaled to match the intensity of the most intense feature in each region. Regions exhibiting obvious discrepancies between the measured and computed IR features are highlighted.

Table 2 Vibrational mode assignments for $[pdThd+H]^+$ and $[pUrd+H]^+$[a]

Vibrational mode assignment	Frequency (cm^{-1}) $[pdThd+H]^+$	$[pUrd+H]^+$
C2═O stretching	1639	
C2═O and nucleobase stretching		1662
Nucleobase stretching	1672	
C4═O stretching	1768	1791
N3–H stretching	3410	3410
O2′–H stretching	—	3588
PO–H and O3′–H stretching	3652	3652

[a] Vibrational mode assignments based on comparison of the measured IRMPD and calculated IR spectra of the **PA** and **PB** conformers of $[pdThd+H]^+$ and $[pUrd+H]^+$.

the **PD**, **PE**, **TB**, **PF**, **TC** and **O4B** conformers of $[pdThd+H]^+$ are compared over the IR fingerprint and hydrogen-stretching regions in Fig. S3 of the ESI.† The IR spectra predicted for these conformers all exhibit obvious discrepancies from the measured IRMPD spectrum, indicating that they are not significant contributors to the experiments. A more detailed discussion is provided in the ESI.†

In summary, comparisons of the measured IRMPD and calculated IR spectra of the low-energy conformers of $[pdThd+H]^+$ indicate that the **PA** and **PB** conformers are predominantly populated in the experiments, a minor population of the **O2A** conformer may also be present. The **PA** conformer found here is consistent with the conformation of $[pdThd+H]^+$ deduced from IMS MS measurements of collision cross section and complementary theoretical modeling.[18] B3LYP predicts **PC** as the ground conformer for $[pdThd+H]^+$. However, the calculated IR spectrum of **PC** exhibits discrepancies with the measured IRMPD spectrum that enable it to be ruled out as an important contributor. Therefore, the relative stabilities of the low-energy conformers of $[pdThd+H]^+$ predicted by MP2 may be more reliable than those of B3LYP. Vibrational mode assignments of $[pdThd+H]^+$ are interpreted primarily based on the calculated IR spectrum of the **PA** and **PB** conformers, and are summarized in Table 2.

Experimental conformations of $[pUrd+H]^+$

The measured IRMPD and calculated IR spectra of the most representative low-energy conformers for each favorable state of protonation, **Pi**, **Pii**, **PA**, **PB**, **PC**, **TA** and **O4A** of $[pUrd+H]^+$ are compared in Fig. 4 over the IR fingerprint and hydrogen-stretching regions. The calculated IR bands that exhibit obvious disagreement with the measured IRMPD bands are highlighted. Similar to that found for $[pdThd+H]^+$, the calculated IR spectra of the **PA** and **PB** conformers of $[pUrd+H]^+$ exhibit excellent agreement with the measured IRMPD spectrum. The calculated IR feature at 3682 cm^{-1}, arising from the hydrogen-bond acceptor O3′H stretching, is shifted relative to the band measured at 3652 cm^{-1}. This shift is due to the anharmonicity of the hydrogen-bonding interaction between the two hydroxyls of the sugar moiety. Therefore, this feature is not diagnostic. Similarly, the hydrogen-bond acceptor O2′H or O3′H stretches predicted at 3685 cm^{-1} for the **Pi** and **Pii** or the **PC** and **TA** conformers, respectively, are again not diagnostic. Although the **Pi** and **Pii** conformers are predicted to be more stable than the **PA** and **PB** conformers, respectively, the bands at 3616 cm^{-1} predicted for the **Pi** and **Pii** conformers are higher in frequency than the measured band at 3588 cm^{-1}. As **Pi** and **PA**, and **Pii** and **PB** differ only differ in the sugar hydroxyl orientation, these rotamers can be differentiated from their IR features. The barriers to interconversion for **Pi** and **PA** and **Pii** and **PB** are predicted to be less than 15 kJ mol^{-1}, and thus these conformers should be able to interconvert at room temperature. The intense anharmonic band predicted at 1579 cm^{-1} for **PC** (dotted line) of $[pUrd+H]^+$ arises from the excess proton oscillating between the phosphate oxo and O2 carbonyl oxygen atoms, which as for $[pdThd+H]^+$ is again not diagnostic. The band predicted at 3635 cm^{-1} for **PC** lies to the red of the measured band at 3652 cm^{-1}. The calculated band at 3570 cm^{-1} of **TA** also lies to the red of the measured band at 3588 cm^{-1}. The calculated band at 1818 cm^{-1} of **O4A** lies to the blue relative to the measured band at 1797 cm^{-1}. The calculated bands above 3550 cm^{-1} of **O4A** exhibit large discrepancies with the measured bands in that region. Therefore, the discrepancies between the measured and calculated spectra of **PC**, **TA**, and **O4A** are sufficient to eliminate these conformers as important contributors to the experimental population. The measured IRMPD and calculated IR spectra of the other stable low-energy conformers of $[pUrd+H]^+$ found (**Piii**, **Piv**, **PD**, **PE**, **TB**, **Ti**, **TC**, **Pv**, **PF**, **Tii**, **O4B**, **O4i**, **Tiii**, and **O2i**) are compared over the IR fingerprint and hydrogen-stretching regions in Fig. S4 and S5 of the ESI.† The discrepancies between the measured and predicted spectra clearly indicate the absence of these conformers in the experimental population. A more detailed discussion is provided in the ESI.†

In summary, comparisons of the measured and calculated IR spectra of $[pUrd+H]^+$ indicate that the **PA** and **PB** conformers are populated in the experiments. Similar to $[pdThd+H]^+$, the B3LYP ground conformer **PC** of $[pUrd+H]^+$ is not present in significant abundance in the experiments, indicating that MP2 theory appears to do a better job at predicting the relative stabilities of the low-energy conformers of $[pUrd+H]^+$. Evident differences between the measured IRMPD and calculated IR spectra particularly in the hydrogen-stretching region for the other low-energy conformers clearly rule out their presence in the experimental population. Vibrational mode assignments of the measured IRMPD spectral features are made based on the calculated vibrational modes of **PA** and **PB** and are summarized in Table 2.

Influence of the phosphate moiety

A variety of 2,4-dihydroxy tautomers of $[dThd+H]^+$ and $[Urd+H]^+$ were found to coexist in the experimental population. Moreover, minor populations of O2 protonated $[dThd+H]^+$ and O4 protonated $[Urd+H]^+$ were also found to contribute to the experiments.[7,8] In contrast, current results for $[pdThd+H]^+$ and $[pUrd+H]^+$ suggest that the **PA** and **PB** conformers are present in the experiments with dominant population. The stable conformers of $[pdThd+H]^+$ and $[pUrd+H]^+$ that dominate the

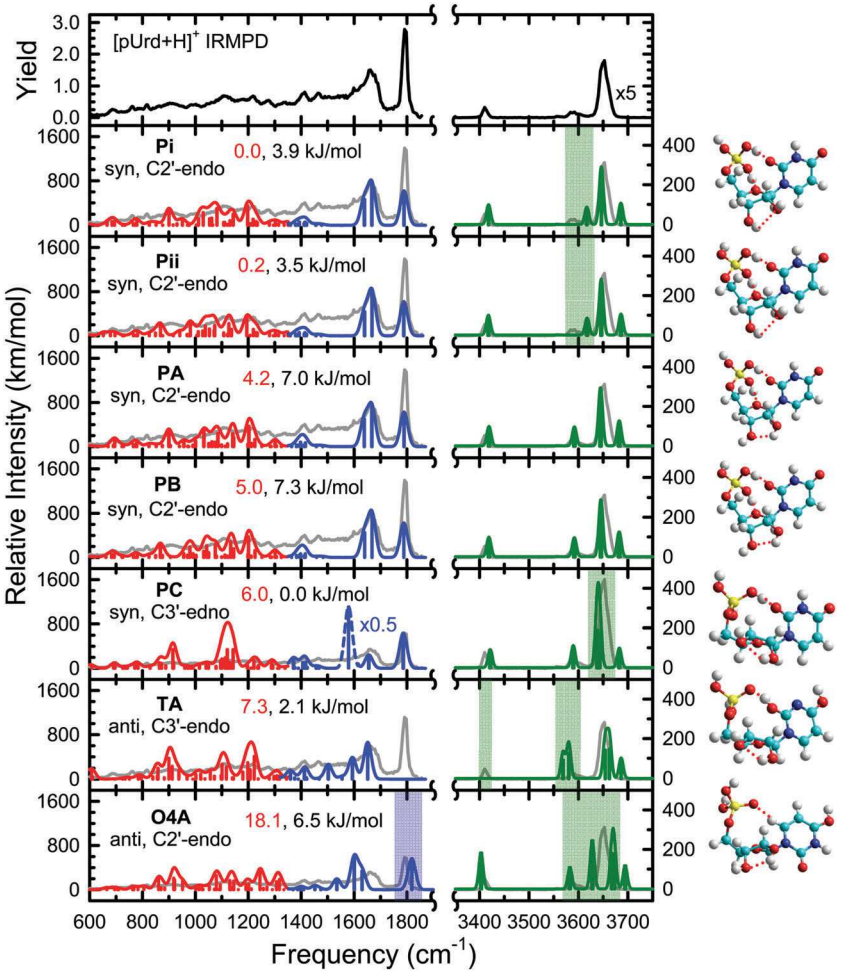

Fig. 4 Comparison of the measured IRMPD action spectrum of $[pUrd+H]^+$ with the calculated IR spectra of the ground and most stable conformers for each protonation site/tautomeric form of $[pUrd+H]^+$ and the corresponding B3LYP/6-311+G(d,p) optimized structures. Also shown are the MP2(full)/6-311+G(2d,2p) (in red) and B3LYP/6-311+G(2d,2p) (in black) relative Gibbs free energies at 298 K. The site of protonation/tautomeric form, nucleobase orientation and sugar puckering are also indicated for each conformer. To facilitate comparison of the measured and calculated spectra, the IRMPD spectrum is overlaid (in grey) with each calculated spectrum and scaled to match the intensity of the most intense feature in each region. Regions exhibiting obvious discrepancies between the measured and computed IR features are highlighted.

experimental population are compared with those of $[dThd+H]^+$ and $[Urd+H]^+$ in Fig. 5. As can be seen, protonation occurs on the phosphate moiety rather than on the nucleobases, and both the Thy and Ura nucleobases remain in their canonical forms in the protonated nucleotides. The protonated phosphate moiety stabilizes *syn* oriented Thy or Ura *via* strong P═$OH^+\cdots$O2 and P–OH$\cdots$O4′ hydrogen-bonding interactions. The strong ionic hydrogen-bonding interaction of the protonated phosphate moiety with the O2 carbonyl of the nucleobase in particular stabilizes the excess proton *via* ion–dipole and ion–induced dipole interactions and thereby impedes tautomerization of the nucleobase that would normally be induced by protonation in the absence of the phosphate moiety. The strong P═$OH^+\cdots$O2 and P–OH$\cdots$O4′ hydrogen-bonding interactions among the phosphate, nucleobase and sugar moieties lead to relatively compact structures and greatly reduce the conformational flexibility of $[pdThd+H]^+$ and $[pUrd+H]^+$. In contrast, for the nucleosides, protonation occurs on the nucleobase and induces tautomerization. The 2,4-dihydroxy nucleobases prefer anti orientations that are stabilized by either a noncanonical C6H$\cdots$O5′ hydrogen bond or a strong O2H$\cdots$O2′H$\cdots$O3′ hydrogen bridge. The IRMPD action spectra of $[pdThd+H]^+$, $[pUrd+H]^+$, $[dThd+H]^+$ and $[Urd+H]^+$ are also compared in Fig. 2. The IRMPD features of $[dThd+H]^+$ and $[Urd+H]^+$ in the fingerprint region are better resolved and more distinguishable than those of $[pdThd+H]^+$ and $[pUrd+H]^+$. The very strong intramolecular hydrogen bonds that stabilize $[pdThd+H]^+$ and $[pUrd+H]^+$ lead to very anharmonic IR vibrations and the extensive broadening observed. In the OPO region, fewer vibrational modes are observed for $[pdThd+H]^+$ and $[pUrd+H]^+$ than for $[dThd+H]^+$ and $[Urd+H]^+$ likely because the strong hydrogen-bonding interactions of $[pdThd+H]^+$ and $[pUrd+H]^+$ lead to gross red shifting of the associated hydrogen-stretching modes (such that they lie outside of the range of vibrational frequencies accessible/examined) and reduced conformational flexibility.

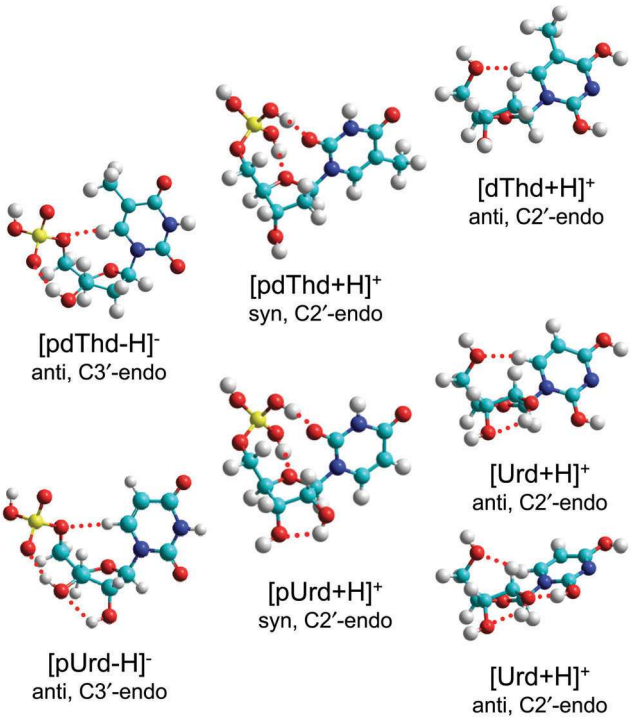

Fig. 5 Comparisons of the stable low-energy conformers of the protonated thymidine and uridine nucleosides, dThd and Urd, and the deprotonated and protonated forms of the thymidine and uridine nucleotides, pdThd and pUrd.

Influence of protonation

The stable conformers of $[pdThd+H]^+$ and $[pUrd+H]^+$ that dominate the experimental population are compared with those found for $[pdThd-H]^-$ and $[pUrd-H]^-$ in Fig. 5. Although the Thy and Ura nucleobase residues of the deprotonated mononucleotides, $[pdThd-H]^-$ and $[pUrd-H]^-$,[15,16] are also found in their canonical form, the nucleobase orientations and sugar puckering are distinctively different from those of $[pdThd+H]^+$ and $[pUrd+H]^+$. In particular, the deprotonated phosphate moieties of $[pdThd-H]^-$ and $[pUrd-H]^-$ form a strong hydrogen-bonding interaction with the 3′-hydroxyl group, and a weak noncanonical hydrogen-bonding interaction with the C6 hydrogen atom of Thy or Ura, which leads to an anti nucleobase orientation and C3′-*endo* sugar puckering. In contrast, $[pdThd+H]^+$ and $[pUrd+H]^+$ adopt a *syn* nucleobase orientation stabilized by strong P═$OH^+\cdots$O2 and P–OH$\cdots$O4′ hydrogen-bonding interactions, resulting in C2′-*endo* sugar puckering. The IRMPD action spectra of $[pdThd+H]^+$, $[pUrd+H]^+$, $[pdThd-H]^-$ and $[pUrd-H]^-$ are compared in Fig. 2. The IRMPD features of $[pdThd-H]^-$ and $[pUrd-H]^-$ are more distinguishable in the fingerprint region than those of $[pdThd+H]^+$ and $[pUrd+H]^+$, again suggesting that the vibrational modes of the protonated species are highly anharmonic due to the nearly equal sharing of the excess proton by the phosphate and nucleobase moieties. Indeed, the 5-methyl substituent of pdThd enhances the relative stability of the O2 protonated conformer such that the anharmonicity should be enhanced and this results in greater IRMPD yield for $[pdThd+H]^+$ than $[pUrd+H]^+$, as observed. Clearly, the local environment is markedly changed by protonation.

Influence of solvent

The lowest energy conformers of $[pdThd+H]^+$ and $[pUrd+H]^+$ computed using the IEFPCM polarizable continuum model corresponding to water are consistent with that found for the isolated species and protonated at the phosphate moiety, the **PA** and **PB** conformers of $[dThd+H]^+$ and the **PA**, **PB**, and **PC** conformers of $[pdUrd+H]^+$. In fact, both MP2 and B3LYP now predict the **PC** conformer as the ground conformer at 298 K (free energy). However, the spectral features of the **PC** conformer are not consistent with the measured IRMPD spectra and thus these conformers are not present in the experimental population. This suggests that if the computed stabilities are reliable that upon desolvation the **PC** conformers undergo a change in sugar puckering from C3′-*endo* to C2′-*endo* to allow formation of a P–OH$\cdots$O4′ hydrogen-bonding interaction to further stabilize these species in the absence of solvent. Consistent with their lack of importance in the experiments, conformers involving canonical forms of the nucleobase protonated at the O2 or O4 positions as well as conformers involving a minor tautomeric form of the nucleobase are destabilized relative to the **PA**–**PC** conformers in a polarizable continuum. Thus, the preferred site of protonation and nucleobase orientation is maintained during the ESI process, and a mixture of phosphate protonated conformers exhibiting a *syn* nucleobase orientation and both C2′-*endo* and C3′-*endo* sugar puckering may be present in solution.

Conclusions

The gas-phase conformations of $[pdThd+H]^+$ and $[pUrd+H]^+$ have been investigated using IRMPD action spectroscopy techniques and theoretical calculations, which reveal that the dominant conformers populated for $[pdThd+H]^+$ and $[pUrd+H]^+$ are protonated at the oxo oxygen atom of the phosphate, **PA** and **PB** conformers, forming strong P═$OH^+\cdots$O2 and P–OH$\cdots$O4′ hydrogen-bonding interactions with the nucleobase and sugar moieties that stabilize a *syn* nucleobase orientation and C2′-*endo* sugar puckering. These findings differ markedly from those of their nucleoside analogues $[dThd+H]^+$ and $[Urd+H]^+$, where a large variety of tautomers and conformers coexist in the experiments.[7,8] The phosphate moiety is the preferred protonation site for pdThd and pUrd, and when protonation does not occur on the Thy or Ura residue, tautomerization is not induced. The strong hydrogen-bonding interactions in $[pdThd+H]^+$ and $[pUrd+H]^+$ lead to very anharmonic vibrational modes particularly in the IR fingerprint region, making the hydrogen-stretching signatures more valuable in determining the populated conformations. Comparison of current results to those of the deprotonated forms of these mononucleotides, $[pdThd-H]^-$ and $[pUrd-H]^-$, reveals the effects of low pH conditions (protonation) on the conformations of pdThd and pUrd. Both the nucleobase orientation and sugar puckering of pdThd and pUrd are altered

under low pH conditions. Because the Thy and Ura residues of $[pdThd-H]^-$ and $[pUrd-H]^-$ remain in their canonical forms, it can be concluded that the presence of the phosphate moiety shuts down nucleobase tautomerization. The stable **PA** conformer of $[pdThd+H]^+$ found here is consistent with the gas-phase conformation of $[pdThd+H]^+$ from IMS MS measurements of collision cross section and complementary theoretical modeling.[18] The consistency found for these two very different approaches to structural characterization validate the present findings. Thus, present results combined with those of parallel studies of the protonated forms of the other DNA and RNA mononucleotides we previously reported find that pdThd and pUrd are the only DNA or RNA mononucleotides that prefer protonation on the phosphate moiety. This observation is consistent with the fact that Thy and Ura have the lowest proton affinities among the nucleobases[67] such that the excess proton attaches to the phosphate oxo oxygen atoms of pdThd and pUrd, whereas the excess proton binds to the nucleobase in the other DNA and RNA mononucleotides.[31,32,34] Thus, protonation along the phosphate backbone will only occur in DNA and RNA oligomers at very low pH and in the absence of adenine, cytosine and guanine residues.

Conflicts of interest

There are no conflicts to declare.

Acknowledgements

Financial support of this work was provided by the National Science Foundation, Grants OISE-0730072, OISE-1357887 and CHE-1709789. R. R. W. also gratefully acknowledges support from a Thomas C. Rumble Graduate Fellowship at Wayne State University. We would also like to thank WSU C&IT for the computational resources and support. This work is part of the research program of FOM, which is financially supported by the Nederlandse Organisatie voor Wetenschappeklijk Onderzoek (NWO). The skillful assistance of the FELIX staff is gratefully acknowledged.

References

1 J. K. Wolken and F. Turecek, *J. Am. Soc. Mass Spectrom.*, 2000, **11**, 1065.
2 E. S. Kryachko, M. T. Nguyen and T. Zeegers-Huyskens, *J. Phys. Chem. A*, 2001, **105**, 1288.
3 J.-Y. Salpin, S. Guillaumont, J. Tortajada, L. MacAleese, J. Lemaire and P. Maitre, *ChemPhysChem*, 2007, **8**, 2235.
4 Y.-w. Nei, T. E. Akinyemi, J. D. Steill, J. Oomens and M. T. Rodgers, *Int. J. Mass Spectrom.*, 2010, **297**, 139.
5 K. T. Crampton, A. I. Rather, Y.-w. Nei, G. Berden, J. Oomens and M. T. Rodgers, *J. Am. Soc. Mass Spectrom.*, 2012, **23**, 1469.
6 J.-Y. Salpin and D. Scuderi, *Rapid Commun. Mass Spectrom.*, 2015, **29**, 1898.
7 R. R. Wu, B. Yang, C. E. Frieler, G. Berden, J. Oomens and M. T. Rodgers, *Phys. Chem. Chem. Phys.*, 2015, **17**, 25978.
8 R. R. Wu, B. Yang, C. E. Frieler, G. Berden, J. Oomens and M. T. Rodgers, *J. Am. Soc. Mass Spectrom.*, 2016, **27**, 410.
9 V. H. Harris, C. L. Smith, W. J. Cummins, A. L. Hamiltion, H. Adams, M. Dickman, D. P. Hornby and D. M. Williams, *J. Mol. Biol.*, 2003, **326**, 1389.
10 M. D. Topal and J. R. Fresco, *Nature*, 1976, **263**, 285.
11 R. R. Wu and M. T. Rodgers, *Phys. Chem. Chem. Phys.*, 2016, **18**, 24451.
12 R. R. Wu, Y. Chen and M. T. Rodgers, *Phys. Chem. Chem. Phys.*, 2016, **18**, 2968.
13 R. R. Wu and M. T. Rodgers, *Phys. Chem. Chem. Phys.*, 2016, **18**, 16021.
14 R. R. Wu and M. T. Rodgers, *Phys. Chem. Chem. Phys.*, 2016, **18**, 24451.
15 Y.-w. Nei, N. Hallowita, J. D. Steill, J. Oomens and M. T. Rodgers, *J. Phys. Chem. A*, 2013, **117**, 1319.
16 Y.-w. Nei, K. T. Crampton, G. Berden, J. Oomens and M. T. Rodgers, *J. Phys. Chem. A*, 2013, **117**, 10634.
17 J.-Y. Salpin, S. Guillaumont, D. Ortiz, J. Tortajada and P. Maitre, *Inorg. Chem.*, 2011, **50**, 7769.
18 J. Gidden and M. T. Bowers, *J. Phys. Chem. B*, 2003, **107**, 12829.
19 B. Chiavarino, M. E. Crestoni, S. Fornarini, F. Lanucara, J. Lemaire, P. Maitre and D. Scuderi, *Int. J. Mass Spectrom.*, 2008, **270**, 111.
20 M. R. Ligare, A. M. Rijs, G. Berden, M. Kabelac, D. Nachtigallova, J. Oomens and M. S. de Vries, *J. Phys. Chem. B*, 2015, **119**, 7894.
21 J. M. Bakker, J.-Y. Salpin and P. Maître, *Int. J. Mass Spectrom.*, 2009, **283**, 214.
22 J. M. Bakker, R. K. Sinha, T. Besson, M. Brugnara, P. Tosi, J.-Y. Salpin and P. Maitre, *J. Phys. Chem. A*, 2008, **112**, 12393.
23 F. Lanucara, M. E. Crestoni, B. Chiavarino, S. Fornarini, O. Hernandez, D. Scuderi and P. Maitre, *RSC Adv.*, 2013, **3**, 12711.
24 G. C. P. van Zundert, S. Jaeqx, G. Berden, J. M. Bakker, K. Kleinermanns, J. Oomens and A. M. Rijs, *ChemPhysChem*, 2011, **12**, 1921.
25 A. Filippi, C. Fraschetti, F. Rondino, S. Piccirillo, V. Steinmetz, L. Guidoni and M. Speranza, *Int. J. Mass Spectrom.*, 2013, **354**, 54.
26 H. U. Ung, K. T. Huynh, J. C. Poutsma, J. Oomens, G. Berden and T. H. Morton, *Int. J. Mass Spectrom.*, 2015, **378**, 294.
27 R. R. Wu, B. Yang, G. Berden, J. Oomens and M. T. Rodgers, *J. Phys. Chem. B*, 2014, **118**, 14774.
28 K. Rajabi, K. Theel, E. A. L. Gillis, G. Beran and T. D. Fridgen, *J. Phys. Chem. A*, 2009, **113**, 8099.
29 R. R. Wu, B. Yang, G. Berden, J. Oomens and M. T. Rodgers, *J. Phys. Chem. B*, 2015, **119**, 2795.
30 R. R. Wu, B. Yang, C. E. Frieler, G. Berden, J. Oomens and M. T. Rodgers, *J. Phys. Chem. B*, 2015, **119**, 5773.

31 R. R. Wu, C. C. He, L. A. Hamlow, Y.-w. Nei, G. Berden, J. Oomens and M. T. Rodgers, *Phys. Chem. Chem. Phys.*, 2016, **18**, 15081.
32 R. R. Wu, C. C. He, L. A. Hamlow, Y.-w. Nei, G. Berden, J. Oomens and M. T. Rodgers, *J. Phys. Chem. B*, 2016, **120**, 4616.
33 B. Yang, R. R. Wu, G. Berden, J. Oomens and M. T. Rodgers, *J. Phys. Chem. B*, 2013, **117**, 14191.
34 R. R. Wu, L. A. Hamlow, C. C. He, Y.-w. Nei, G. Berden, J. Oomens and M. T. Rodgers, *J. Am. Soc. Mass Spectrom.*, 2017, **28**, 1638.
35 J. Oomens, A. R. Moehlig and T. H. Morton, *J. Phys. Chem. Lett.*, 2010, **1**, 2891.
36 E. A. L. Gillis, K. Rajabi and T. D. Fridgen, *J. Phys. Chem. A*, 2009, **113**, 824.
37 E. A. L. Gillis, M. Demireva, K. Nanda, G. Beran, E. R. Williams and T. D. Fridgen, *Phys. Chem. Chem. Phys.*, 2012, **14**, 3304.
38 M. Azargun and T. D. Fridgen, *Phys. Chem. Chem. Phys.*, 2015, **17**, 25778.
39 C. M. Kaczan, A. I. Rathur, R. R. Wu, Y. Chen, C. A. Austin, G. Berden, J. Oomens and M. T. Rodgers, *Int. J. Mass Spectrom.*, 2015, **378**, 76.
40 B. Yang, R. R. Wu, N. C. Polfer, G. Berden, J. Oomens and M. T. Rodgers, *J. Am. Soc. Mass Spectrom.*, 2013, **24**, 1523.
41 J.-Y. Salpin, V. Haldys, S. Guillmont, J. Tortaada, M. Hurtado and A. Lambashi, *ChemPhysChem*, 2014, **15**, 2959.
42 Y. Zhu, L. A. Hamlow, C. C. He, S. F. Strobehn, J. K. Lee, J. Gao, G. Berden, J. Oomens and M. T. Rodgers, *J. Phys. Chem. B*, 2016, **120**, 8892.
43 Y. Zhu, L. A. Hamlow, C. C. He, J. K. Lee, J. Gao, G. Berden, J. Oomens and M. T. Rodgers, *J. Phys. Chem. B*, 2017, **121**, 4048.
44 Y. Zhu, L. A. Hamlow, C. C. He, H. A. Roy, N. A. Cunningham, M. U. Munshi, G. Berden, J. Oomens and M. T. Rodgers, *Int. J. Mass Spectrom.*, 2017, DOI: 10.1016/j.ijms.2017.04.005.
45 Y. Zhu, H. A. Roy, N. A. Cunningham, S. F. Strobehn, J. Gao, M. U. Munshi, G. Berden, J. Oomens and M. T. Rodgers, *Phys. Chem. Chem. Phys.*, 2017, **19**, 17637.
46 Y. Zhu, H. A. Roy, N. A. Cunningham, S. F. Strobehn, J. Gao, M. U. Munshi, G. Berden, J. Oomens and M. T. Rodgers, *J. Am. Soc. Mass Spectrom.*, 2017, **28**, 2423.
47 B. Power, V. Haldys, J.-Y. Salpin and T. D. Fridgen, *J. Mass Spectrom.*, 2016, **51**, 236.
48 B. Power, S. Rowe and T. D. Fridgen, *J. Phys. Chem. B*, 2017, **121**, 58.
49 M. Azargun, Y. Jami-Alahmadi and T. D. Fridgen, *Phys. Chem. Chem. Phys.*, 2017, **19**, 1281.
50 J. J. Valle, J. R. Eyler, J. Oomens, D. T. Moore, A. F. G. van der Meer, G. von Heldon, G. Meijer, C. L. Hendrickson, A. G. Marshall and G. T. Blakney, *Rev. Sci. Instrum.*, 2005, **76**, 023103.
51 N. C. Polfer, J. Oomens, D. T. Moore, G. von Helden, G. Meijer and R. C. Dunbar, *J. Am. Chem. Soc.*, 2006, **128**, 517.
52 N. C. Polfer and J. Oomens, *Phys. Chem. Chem. Phys.*, 2007, **9**, 3804.
53 D. Oepts, A. F. G. van der Meer and P. W. van Amersfoort, *Infrared Phys. Technol.*, 1995, **36**, 297.
54 K. Wolinski, J. F. Hinton, D. S. Wishart, B. D. Sykes, F. M. Richards, A. Pastone, V. Saudek, P. D. Ellis, G. E. Maciel, J. W. McIver, A. C. Blizzard, D. P. Santry, J. A. Pople, N. S. Ostlund, L. Ducasse, J. Hoarau, M. Pesquer, M. Kondo, I. Ando, R. Chujo, A. Nishioka, E. C. Vauthier, S. Odiot, F. Tonnard, J. D. Baker, M. C. Zerner, D. V. Beveridge, W. P. Anderson, T. R. Cundari, R. C. Bingham, M. J. S. Dewar, D. H. Lo, J. Li, P. C. Mello, K. Jug, W. Tihiel, E. G. Zoebisch, E. F. Healy, J. J. P. Stewart, M. Fraser and D. M. Hayes, *HyperChem Computational Chemistry Software Package, Version 8.0*, Hypercube, Inc., Gainsville, FL, 2007.
55 M. J. Frisch, G. W. Trucks, H. B. Schlegel, G. E. Scuseria, M. A. Robb, J. R. Cheeseman, G. Scalmani, V. Barone, B. Mennucci, G. A. Petersson, H. Nakatsuji, M. Caricato, X. Li, H. P. Hratchian, A. F. Izmaylov, J. Bloino, G. Zheng, J. L. Sonnenberg, M. Hada, M. Ehara, K. Toyota, R. Fukuda, J. Hasegawa, M. Ishida, T. Nakajima, Y. Honda, O. Kitao, H. Nakai, T. Vreven, J. A. Montgomery, Jr., J. E. Peralta, F. Ogliaro, M. Bearpark, J. J. Heyd, E. Brothers, K. N. Kudin, V. N. Staroverov, R. Kobayashi, J. Normand, K. Raghavachari, A. Rendell, J. C. Burant, S. S. Iyengar, J. Tomasi, M. Cossi, N. Rega, J. M. Millam, M. Klene, J. E. Knox, J. B. Cross, V. Bakken, C. Adamo, J. Jaramillo, R. Gomperts, R. E. Stratmann, O. Yazyev, A. J. Austin, R. Cammi, C. Pomelli, J. W. Ochterski, R. L. Martin, K. Morokuma, V. G. Zakrzewski, G. A. Voth, P. Salvador, J. J. Dannenberg, S. Dapprich, A. D. Daniels, Ö. Farkas, J. B. Foresman, J. V. Ortiz, J. Cioslowski and D. J. Fox, *Gaussian 09, Revision C.01*, Gaussian, Inc., Wallingford, CT, 2009.
56 J.-Y. Salpin, L. MacAleese, F. Chirot and P. Dugourd, *Phys. Chem. Chem. Phys.*, 2014, **16**, 14127.
57 B. Chiavarino, M. E. Crestoni, S. Fornarini, D. Scuderi and J.-Y. Salpin, *Inorg. Chem.*, 2015, **54**, 3513.
58 S. Katsyuba and E. Vandyukova, *Chem. Phys. Lett.*, 2003, **377**, 658.
59 J. O. Jensen, A. Banerjee, D. Zeroka, C. N. Merrow, S. J. Gilliam and S. J. Kirkby, *Spectrochim. Acta, Part A*, 2004, **60**, 1947.
60 D. Scuderi, C. F. Correia, O. P. Balaj, G. Ohanessian, J. Lemaire and P. Maitre, *ChemPhysChem*, 2009, **10**, 1630.
61 B. S. Fales, N. O. Fujamade, Y.-w. Nei, J. Oomens and M. T. Rodgers, *J. Am. Soc. Mass Spectrom.*, 2011, **22**, 81.
62 B. S. Fales, N. O. Fujamade, J. Oomens and M. T. Rodgers, *J. Am. Soc. Mass Spectrom.*, 2011, **22**, 1862.
63 D. T. Moore, J. Oomens, L. van der Meer, G. von Helden, G. Meijer, J. Valle, A. G. Marshall and J. R. Eyler, *ChemPhysChem*, 2004, **5**, 740.

64 N. Heine, M. R. Fagiani, M. Rossi, T. Wende, G. Berden, V. Blum and K. R. Asmis, *J. Am. Chem. Soc.*, 2013, **135**, 8266.
65 T. E. Cooper, J. T. OBrien, E. R. Williams and P. B. Armentrout, *J. Phys. Chem. A*, 2010, **114**, 12646.
66 C. S. Contreras, N. C. Polfer, J. Oomens, J. D. Steill, B. Bendiak and J. R. Eyler, *Int. J. Mass Spectrom.*, 2012, **330-332**, 285.
67 E. P. Hunter and S. G. Lias, *J. Phys. Chem. Ref. Data*, 1998, **27**, 413.
68 G. C. Pimentel and A. L. McClellan, *The Hydrogen Bond*, W. H. Freeman, San Francisco, 1960.
69 E. S. Stoyanov, *Phys. Chem. Chem. Phys.*, 2000, **2**, 113.
70 E. S. Stoyanov, *Phys. Chem. Chem. Phys.* 2000, **2**, 1137.